Article:

Abuan, B. and Howell, R.J. orcid.org/0000-0002-0142-9728 (2019) The performance and hydrodynamics in unsteady flow of a horizontal axis tidal turbine. Renewable Energy, 133. pp. 1338-1351. ISSN 0960-1481

https://doi.org/10.1016/j.renene.2018.09.045

The Performance and Hydrodynamics in Unsteady Flow of a Horizontal Axis Tidal Turbine

Binoe E. Abuan[1], Robert J. Howell[2]
University of the Philippines, Diliman, Quezon City
University of Sheffield, Sheffield, United Kingdom

ABSTRACT

This paper presents the effect of idealised unsteady tidal velocities on the performance of a newly-designed Horizontal-Axis Tidal Turbine (HATT) through the use of numerical simulations using Computational Fluid Dynamics (CFD). Simulations are conducted using ANSYS FLUENT implementing the Reynolds-Averaged Navier Stokes (RANS) equations to model the fluid flow problem. A steady flow case is modelling in a 2 m/s stream flow and the resulting performance curve was used as the basis of comparison for the unsteady flow simulations. A decrease in performance was seen for the unsteady flow simulation around peak TSR (TSR=6) which has a cyclic-averaged coefficient of performance (CP) of 37.50% compared to the steady CP of 39.46%. Similar decreases in performance with unsteady flow was observed away from the peak performance TSR at TSR=4 and TSR=8. Furthermore, with unsteady flow that it was found that as the TSR increases, the difference between the cyclic-averaged CP and the steady flow CP drops. The effect of variations in the frequency and amplitude of the unsteady flow showed that a decrease in the cyclic-averaged CP was observed and this performance reduced with increasing frequency and increasing amplitude of unsteady incoming flows. For the cases studied here, unsteady flows are detrimental to the performance of the tidal turbine.

Keywords - Horizontal Axis Tidal Turbine (HATT); unsteady flow; hysteresis curve; Coefficient of Performance (CP); Computational Fluid Dynamics (CFD).

1. INTRODUCTION

Tidal energy is one of the less developed renewable energy source but one that has significant potential for large scale energy generation given the world's tidal capacity is around 120 GW. In the UK alone, the expected capacity is expected to exceed 10GW which is about 50% of Europe's total tidal capacity [1] but despite this potential, the technology is still in its pre-commercialisation stage. Tidal energy is still years behind wind energy in terms of energy produced [2]. In the UK, tidal power is only 0.5% of the country's total power generated and is only 1% of electricity harnessed from renewable energy [3].

The horizontal axis tidal turbine (HATT) is an energy extraction device very similar to horizontal axis wind turbine (HAWT) in terms of functions and components although additional considerations are necessary for tidal blade designs since it will be submerged under water. HATT's will turn slower because water flow velocities are lower than typical wind speeds [4]. Other differences includes higher axial thrust loads, cavitation, potentially higher unsteady blade loading, and a requirement for blade surface treatments against bio-fouling.

Currently installed HATTs include the 500 kW Deepgen tidal stream turbine by Tidal Generation Limited (TGL) which is successfully installed in the EMEC's site at the fall of Warness at Eday in 2010. Alstom acquired TGL in 2013 and they developed a 1 MW turbine in a project called ReDAPT (Reliable Data Acquisition Platform for Tidal) which aims to collect and publish data for tidal energy production for an 18 month period. General Electric (GE) acquired Alstom tidal in 2016 and currently planning to produce the next generation 1.4 MW Oceade Tidal Turbine [4]. Other projects include Aquamarine's 2.4 MW tidal stream turbine called Neptune and Atlantis Resources Limited's Meygen project which have deployed their first Andritz Hydro Hammerfest turbine at full power in December, 2016. Marine Current Turbines also have their twin turbines called SeaGen which was tested in December 2008 and is able to produce 1.2 MW per turbine at a tidal current velocity of 2.4 m/s.

1.1 Steady Flow Simulations and Experiments

Steady flow performance and blade loading has been presented in a number of different published studies. Bahaj et al [5] undertook a number of experiments both in a cavitation tunnel and a towing tank which were used as validation for numerical modelling with Blade-Element Momentum (BEM) method and Computational Fluid Dynamics (CFD) simulations. Small scale experimental modelling to observe wake meandering has been carried out by Chamorro et al [6] using 3D Particle Image Velocimetry (PIV) in an open channel experiment. Walker, in his PhD study at Sheffield, looked at the effects of support structure interference on HATT performance using a circulating water flume [7] while Morris [8] examined solidity, wake recovery and blade deflection using a water flume.

In terms of numerical modelling, BEM and Reynolds-averaged Numerical Simulation (RANS) CFD simulations with Large Eddy Simulation (LES) are the ones being used for most numerical studies. The BEM method has been explored and validated by Bahaj and Batten et al [9] with the use of their experimental results in a cavitation tunnel and towing tank and was proven to be effective in exploring performance curve in tidal turbines. BEM has also been integrated into wind and tidal turbine performance and design software and includes Gerrand Hassan's Bladed and Tidal Bladed has been validated by the Energy Technological Institute (ETI) as well as Batten et al. [9] QBlade is a BEM based open source software used and validated by the authors for use in tidal turbines [10, 11].

Although BEM has been widely used in tidal turbine design and analysis it has limitations. To overcome these limitations, CFD (RANS and others) has been used and developed. Malki et al [12] used a coupled BEM-CFD model to address the limitation of BEM but still have faster simulations than CFD. Investigations of wakes has been carried out by MacLeod et al [13] using a RANS solver with k-ε turbulence closure model and has found that 5D separation is enough for tidal turbines in an array as the velocity/energy is recovered at this distance. RANS is also been used for the investigation of solidity and blade deflection by Morris [8] while the effect of plug flow and high shear flow to tidal turbine was investigated by Mason-Jones et al [14] using RANS with a very similar model used by O'Dohetry et al. [15] when they looked at the feasibility of tidal turbine sites in the Welsh coast.

Afgan et al [16] looked at blade loading and turbulence in tidal turbine using both RANS and LES and compared the two CFD models and compared it using the experimental results by Bahaj et al [9]. It was found that LES provides greater insight into flow physics especially at low TSR at the expense of higher computational time. Kang et al [17] used LES to look at an isolated rotor versus a full tidal turbine model. It was stated that in terms of power coefficients, the results from the two simulations are very similar which means that the pressure fields in the turbine blades which generate torques from extracting power from the current is not significantly affected by the other parts of the turbine.

1.2 Unsteady Flow Simulations and Experiments

Tidal turbine performance and hydrodynamics has been studied for steady flow but there is very little published when incoming flows are unsteady and more research is necessary. The authors can find no literature using RANS CFD models, as used here, to investigate the effects of unsteady flow on the power generating performance of turbines and the underlying aerodynamics, although lots of work has been carried out on other aspects, such as FSI, loading, noise generation etc. Studies using BEMs have however been carried out, for example, O'Rourke et al [18] used a unsteady BEM to investigate the unsteady flow that results due to current shear and yaw misalignment showing they have a significant impact on the hydrodynamic performance of a tidal current turbine. Ai et al [19] showed that unsteady flow due to long waves, introduce non-linearity in the response of the turbine particularly at low tip speed ratio as well as can affecting the time-averaged power coefficient. While such studies are useful, they are limited in the flow physics that can be extracted from them and illustrate why the work in this paper is required. A study done by Leroux, et al [20] uses realistic unsteady inflow from tidal streams in Nova Scotia and looks at its effects in tidal turbine performance. The results show a maximum difference of 0.83% between steady and unsteady values for a stream with a 2.05 m/s average speed and an average amplitude of 10%. While the performance report is presented, the hydrodynamics explaining what happened is not included in the paper because it is too complex to explain without looking at basic unsteady flow effects first which is what the authors want to present in this paper.

Most of the current research for tidal turbines in unsteady flow looks at blade (thrust) loading. The reason is that fatigue loading in unsteady flow is one of the underestimated effects of unsteadiness that is needed to be considered in blade and rotor design. Young et al [24] has shown using BEM-FEM solver that at highly-loaded off-design measurements, the maximum von Mises stress exceeds the design material's yield strength by 65% when compared to steady flow blade loading, suggesting the same effect to the blade through fatigue loading. De Jesus Henriques et al [21] showed, using experimental models, that changes in blade pitch angle could be used as a mechanism for reducing the loading on a HATT when operating with unsteady flows driving excessive wave-induced loads, while still enabling a significant amount of the available power in the unsteady tidal stream to be extracted

Three phenomenon related to blade loading have been mentioned in the literature – added mass, dynamic inflow, and dynamic stall. The effect of added mass has been investigated by Miniaci et al [25] using aerodynamic analysis program (FAST and AeroDyn) and they found that there is a significant effect on blade loading. However, results from Whelan et al [22] showed the opposite where effects from axial added mass of rotor operating in a mean current subjected to passing waves was shown to be small and indeed insignificant. Whelan [26] states that for quick changes in velocity, it was found that the greater flow field cannot respond quickly enough to establish steady state conditions and an overshoot in the blade loading were observed. Planar oscillatory experiments conducted by Milne et al [23] shows that there is an increase in blade loads with increased frequency and loads exceeded the steady state blade loads by up to 15% for reduced frequencies between 0.03 and 0.10 with maximum unsteady amplitude of 25%. A phase lead of the blade loads over velocity was also observed, which is also an expected effect from dynamic inflow. It was also found that the amplitudes of multi-frequency loading can be modelled using superposition which will be important in the design stage of tidal turbines to investigate fatigue loads. For lower TSR, delayed separation, phase lag and dynamic stall were observed. These result to exceeding the steady loading by up to 25% while exhibiting a large degree of hysteresis. [27] Dynamic stall is defined as the result of unsteady and/or fluctuating time histories which leads to a variation in velocity over the turbine rotor. This results to changes in lift and drag coefficients due to flow separation around the foil which is dependent on the time-dependent changes in angle of attack. Dynamic stall also results to overshoots in load magnitudes over steady flow values and induces hysteresis. Dynamic inflow phenomenon in oscillating aerofoil was presented by Lee and Gerontakos [28] while Leishman [29] explained the phenomenon in helicopter and wind turbine settings. Dynamic stall phenomenon at low TSR in tidal turbine under unsteady flow is also presented in Milne et al [23] study when they explains hysteresis curve variation when frequency of the forcing velocity was changed.

Galloway [31] conducted a study on the effects of waves and misaligned flow and found out that wave effects are not significant in terms of power output of the turbine but is significantly affecting blade loading due to the cycling loading resulting into fatigue in blades. Luznik et al [32] conducted an experiment in a three-bladed HATT with and without waves to look at the effects of waves in performance. Results suggest that the effect of waves is insignificant, for the conditions used, as the values of CP with waves shows similar results with steady data.

Current literature does not include much information regarding the effects of flow unsteadiness on performance of HATTs. This paper aims to start to fill that gap by investigating the effects of frequency and amplitude variations on the performance of a newly designed HATT with a detailed explanation of the hydrodynamics that cause that change in performance.

2. TEST CASE AND METHODOLOGY

The tidal turbine that will be used here was designed at the University of Sheffield with the blade specifications described in Table 1. The design process and structural analysis for the turbine is presented in previous papers by the author [10, 11, 35]. The Sheffield HATT was designed using QBlade to have a high CP over a wide range of TSRs so as to be used as a reference case when comparing unsteady flow results.

Table 1

Sheffield HATT Geometry Specifications

Radial Position (m)	Chord Length (m)	Twist (°)	Foil Profile
0.4	0.25	20	NACA 4424
0.6	0.2312	14.5	NACA 4420
0.8	0.2126	11.1	NACA 4418
1.0	0.1938	8.9	NACA 4417
1.2	0.175	7.4	NACA 4416
1.4	0.1562	6.5	NACA 4415
1.6	0.1376	5.9	NACA 4414
1.8	0.1188	5.4	NACA 4413
2.0	0.1	5	NACA 4412

A CFD model of the Sheffield HATT geometry was created using the meshing software ANSYS ICEM-CFD. A mesh independence study and a boundary size study were conducted to determine the most suitable mesh to be used for the CFD simulations, see Abuan et al [11]. An unstructured tetrahedral mesh with 300 cells at the 75% span of the blade with 15 layers of prism cells was chosen in the mesh independent study which is presented in Figure 1a in a cut plane view. The computational domain and boundary conditions was illustrated in Figure 1b, it should be noted that the boundary conditions for the top part of domain was also set as wall and not free-surface with the reason being that the mesh was also intended to be used to validate experimental data from a cavitation tank/wind tunnel. Figure 1c shows the entirety of the rotational part of the domain. It was shown in Abuan [11] the complete basis of the domain size for both the rotational and stationary part which is mainly based on the distance by which the rotational domain is not affecting the flow and is resolved in the simulation. The author also choose not to include the hub of the rotor as its effects is minimal based on the study by Kang et al [17] where they compared full tidal turbine performance to a blade only model and negligible differences were presented.

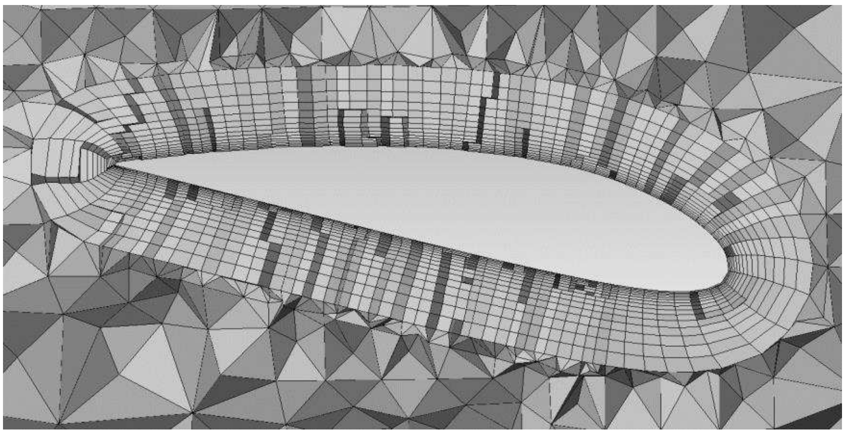

(a)

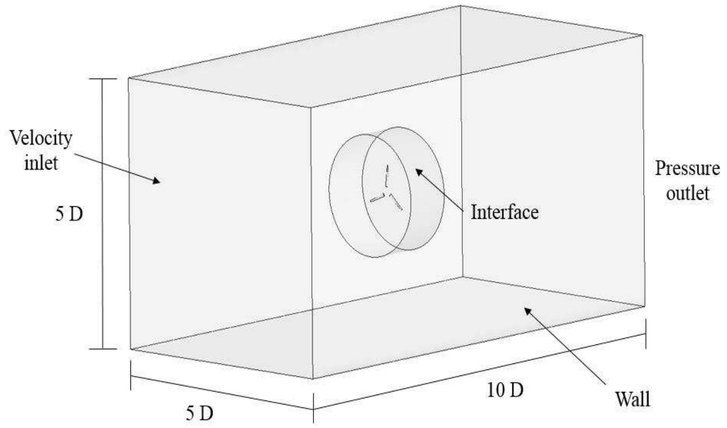
Velocity
inlet
5 D
Interface
Pressure
outlet
Wall
10 D
5 D

(b)

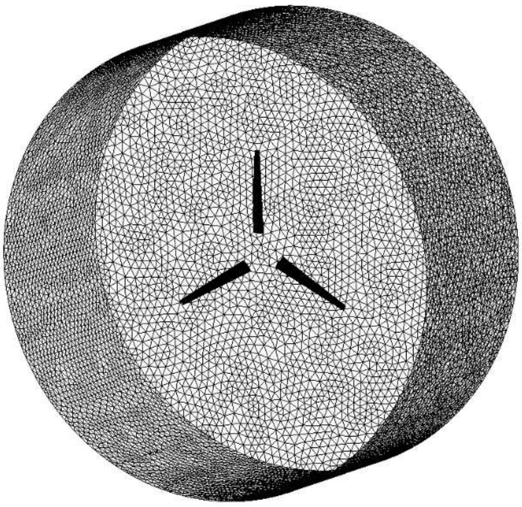

(c)

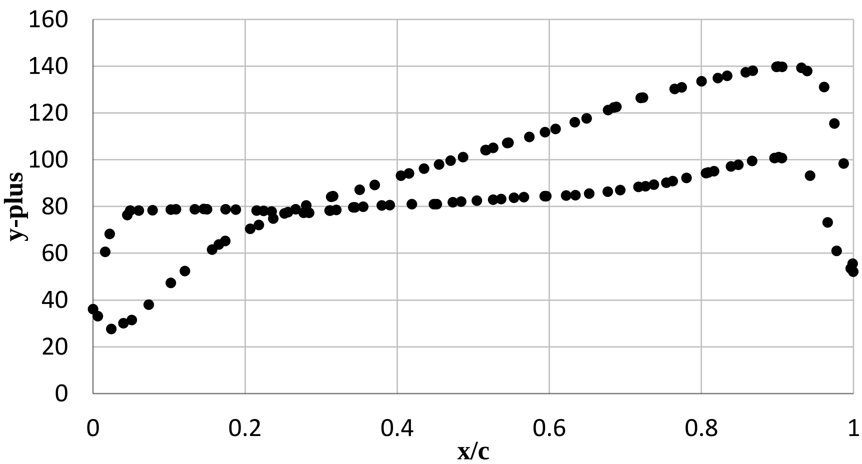
y-plus
x/c
0
20
40
60
80
100
120
140
160
0
0.2
0.4
0.6
0.8
1

(d)

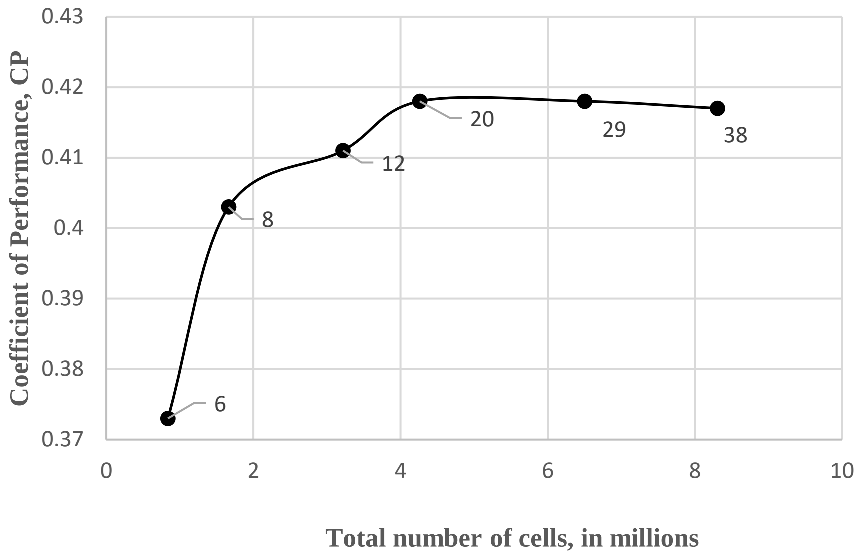

(e)

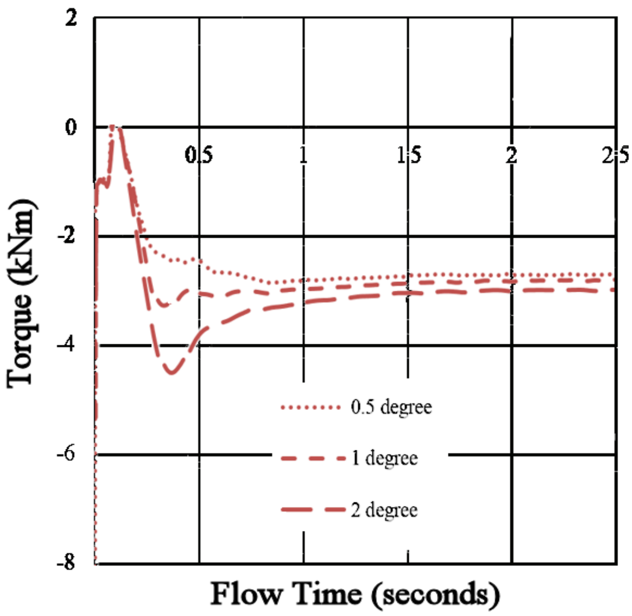

(f)

Figure 1 Sheffield HATT mesh information and images; cut plane to show prism layer boundary mesh (a) whole computational domain showing boundary conditions (b) the rotational domain (c) , y-plus values plot near mesh at 75% span (d) together with the results of the mesh independence study (e) and time independence study (f) for the Sheffield HATT model

Studies were carried out to ascertain the quality of the simulations. These include a mesh independence study, effect of boundary size, turbulence model and time-step. The data for these are presented and are available in the author's previous work and freely available [10, 11, 31]. Figure 1e and Table 2 show the mesh independence study carried out by the authors in previous work where the turbine performance was used as the measurement metric at a TSR of 6 for different mesh sizes. Mesh 4 was selected as it shows very close CP values to that of the denser meshes but requires less computational hours. The numbers behind the points in Figure 1 are the computational hours it needs for the simulation to converge. We can see mesh 4, the one with 20 hour computing time, to have very similar CP values with meshes 5 and 6 with significant difference in computing time. Simulations were conducted using

ANSYS FLUENT's Reynolds-Averaged Navier Stokes (RANS) method with the k-ω SST as the closure turbulence model with y+ values at the log layer between 30 and 100 as can be seen in Figure 1d where the y-plus values near the wall at the 75% span cross section is presented. Figure 1f shows the results of a study into the effects of time-step interval on the solution. This showed that the turbine torque differed by just 1% between the one degree per time-step simulation and a 0.5 degree per time step simulation. The latter is considerably more demanding in computational time and as a result a 1 degree time step was chosen for this study. The water flow velocity for this study was set to 2 m/s which is within the range of optimum velocity for tidal turbines as quoted from Carbon Trust [33] and corresponds to a Reynolds number of 1,350,000 at the 75% span of the blade. Second-order transient implicit formulation was chosen to assure convergence but with more iterations per time-step (30 iterations per time step was used for this study as determined in previous studies by Danao and Abuan [10, 35]) and since the mesh was made using unstructured tetrahedrals and the mesh grid is not aligned to the flow, the second-order upwind discretisation scheme were used for improved accuracy at the expense of slightly longer computational time. Solutions were deemed to have converged when residual values reached 5 x 10^{-5}. Periodic convergence (shown later) was achieved after around 10 rotations of the turbine.

Table 2
Mesh Independence Study Results for the Sheffield HATT at water velocity=2m/s and TSR=6

Mesh no.	Target no. of Cells at 0.75 span	Total no. of cells	Coefficient of Performance	Computational time (at 48 cores, hours)
1	50	836,654	0.373	6
2	100	1,661,936	0.403	8
3	200	3,217,579	0.411	12
4	300	4,259,402	0.418	20
5	350	6,500,103	0.418	29
6	400	8,308,612	0.417	38

The predicted power curves from both the CFD simulation initial BEM results from QBlade are presented in Figure 2. Both curves display similar shape and trends with maximum CP occurring close to TSR=6. The computation of CP used for the steady flow simulations is derived from standard practices presented in current literature [5, 23, 27] where the CP is the ratio of the power extracted by the turbine to the power available in the water flow. The CFD simulation however has a lower power but this is due to the three dimensional effects that are not modelled in the BEM.

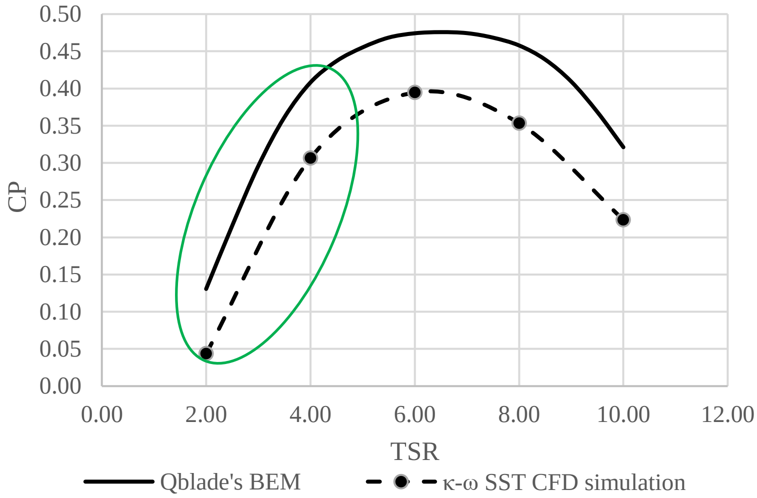

Figure 2 Power curve comparison between CFD and BEM results for the Sheffield HATT.

Low performance (power generation) is observed at low TSRs where high angles of attack are generated; this will generate higher lift but also high drag and possibly separated flows that causes high form drag. Figure 3 shows the streamlines at the 25% and 75% span of the blade for TSR=2 where a large separation in the suction side of the blade surface is observed. As the TSR increases, the angle of attack will decrease which results to two phenomena. First is the decrease in lift but also flow reattachment and so lower drag. This is observed in the region in Figure 2 highlighted with the green oval. The decrease in drag is greater than the decrease in lift caused by the decrease in AoA thus resulting to an increase in lift to drag ratio and hence CP.

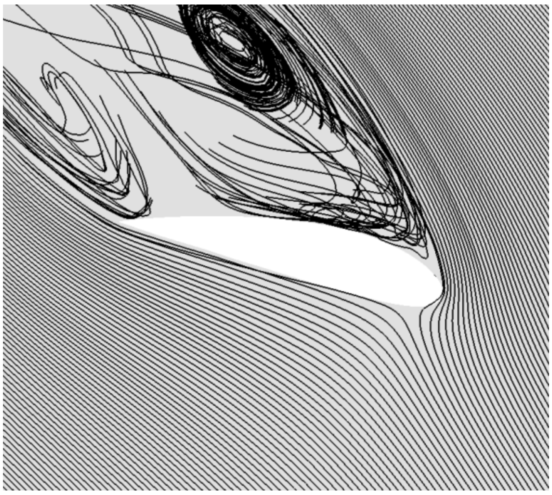

(a)

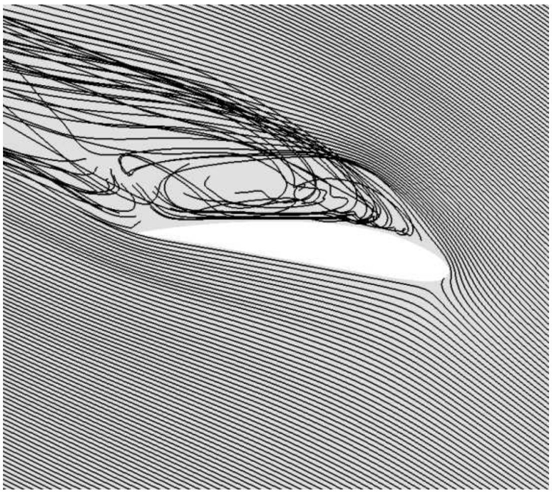

(b)

Figure 3 Streamlines at the 25% (a) and 75% (b) blade span at TSR=2 for the Sheffield HATT steady simulation.

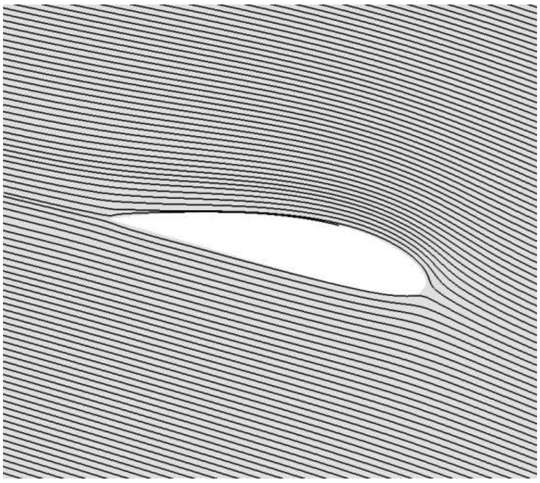

Figure 4 Streamlines at the 75% blade span at TSR=4 for the Sheffield HATT steady simulation.

Performance reached its maximum at TSR=6 with a CP value of 39.46% where the turbine has an optimum combination of lift and drag. Figure 4 illustrates the streamlines around a hydrofoil cross-section at 75% blade span and it can be seen that the flow is fully attached eliminating the effect of additional drag thus making CP higher. After this point, the CP started decreasing at higher TSRs, because the incident AoA decreases thus resulting in lower lift. Drag will not change much at high TSRs because the AoA is tends to zero meaning that CP is more dominated by the sensitivity to changes in lift. Negative-lift is also observed at TSR=10 where there is an overlap in the lines of pressure coefficient as shown in Figure 5, and this also contributes to the lower power observed.

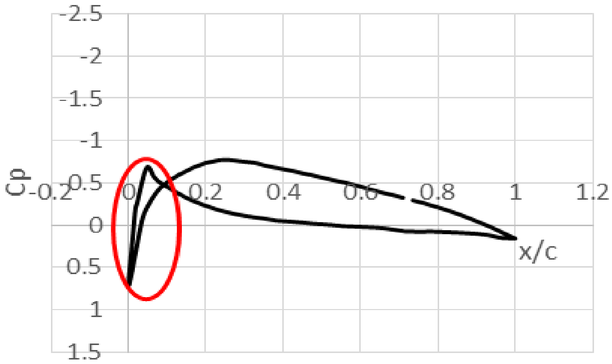

Figure 5 Coefficient of pressure plot across the 75% blade span at TSR=10 for the Sheffield HATT steady simulation.

3. RESULTS AND DISCUSSION

3.1 Unsteady Flow Simulation

The peak of the power curve (CP=39.5%) at TSR=6 was chosen to be the reference point for comparison with the unsteady flow simulations since any turbine would generally be operated at the location of maximum performance. The idealised unsteady flow velocity was set to have amplitude of 25% of the mean velocity. Frequency of the fluid flow was set to produce a flow frequency of 1 Hz and this was defined to be the unsteady base case since other unsteady results will be compared to this. To achieve this, a User Defined Function (UDF) was created, which defined the velocity at the inlet boundary of the computational domain to vary with time using the equation $u(t) = 1.94 + 0.49\ sin(2\pi t)$, where t is the flow time in seconds. It is important to note that this equation was also set to have a cyclic-averaged water power equal to that of a steady flow at 2 m/s.This frequency corresponds to a Leishman’s reduced frequency (k) of 0.051 which is just outside the quasi-steady flow range defined to be values of k between 0 and 0.05.

The unsteady simulation was conducted using the same settings and mesh used for the steady-state simulation and the results were monitored per time-step to present a whole cycle response of the turbine. The time-step used for this study is set as the time it needs for the rotor to move 1º, this was chosen as a result of the time-step study where two more time-steps were considered – one time-step for 0.5˚ and one time-step for 2.0˚. Independence of the solution t the time step was achieved with a time step of 0.00299 s, equivalent to a rotation of 1°. To achieve cycle-converegene, the turbine is allowed to run for more than 10 complete flow cycles. Figure 6a presents the instantaneous Power Extracted (Pe) by the turbine together with the Power Available (Pa) and the unsteady velocity with time, this is a full cycle after cycle-convergence is converged as shown in Figure 6b. The interaction of the two curves (Pe and Pa) resulting to the instantaneous CP presented in Figure 7 together with the instantaneous TSR, which is a one cycle of what is being shown in Figure 6b. The cyclic-averaged CP, defined to be the ratio of the averaged Pe and averaged Pa, for this unsteady simulation is 37.5%. This definition was used in order to have direct comparison with the steady flow simulations since it was intended that the averaged water power avaialable for the unsteady cases should be equal to the power available at the same TSR. This is 1.94% lower than that of the steady-state CP at TSR=6. From this data alone, it can be said that the presence of the unsteadiness of the flow results to a decrease in CP alone which also mean that there is a decrease in the averaged power extracted since the averaged power available for the unsteady simulation was maintained to be the same to that of the steady-state water power. From the instantaneous power plots in Figure 6, it can be seen that there is a lag observed for the instantaneous Pe with respect to the instantaneous Pa accounting to 2.8% of the normalised flow time. This lag results on a delay on the increase of the instantaneous CP whereas a very slow increase was found out between points **a** and **b** as shown in Figure 7. As the time progress, a steeper increase in the instantaneous CP curve was found on the region fromed by the points **b**, **c** and **d** (highlighted by a red oval) with a maximum CP of 42.2%. Again, this is caused by the lag found on the instantaneous power extracted by the turbine whereas a higher Pe that is only dropping at this point is paired with an already dropped water power thus increasing the CP. At τ=0.528, Pe goes back to its initial value and started to decrease in value while the Pa curve is already decreasing starting from τ=0.50, as a result, a steep drop in CP value was observed as shown in Figure 7 highlighted by a green oval. The decrease in CP was observed until τ=0.796 with a lowest CP of 28.9% It can also be observed that the steepness of the decreasing Pe curve is less than that of the Pa curve which means that there is slower decrease in the numerator of the CP ratio thus resulting to the steep decrease. A fast recovery of the CP value was observed past the lowest point at τ=0.796 at τ=1.0.

Anotherway to present the instantaneous CP curve for the turbine is to present it as a so-called hysteresis curve, superimposed on the steady state power curve as shown in Figure 8. The hysteresis curve also shows that the cycle is completed and cycle-convergence is achieved because the curve is continuous. A break in the line occurs if cperiodic convergence is not achieved. It is clearly illustrated how the unsteadiness of the flow affects the performance of the turbine through the hysteresis curve does not follow the steady state curve. Segments of the hysteresis curve defined by the region **b-c-d-e** have a CP value higher than their steady state counterpart, while the region **f-g-h-a** has lower CP value. The steep decrease was also observed at high TSR which can be attributed to the sensitivity of the changes in lift and hence lift to drag ratio in the hydrofoils used at low AoA which is present at high TSR. The lift to drag ratio of the blade at 25% and 75% of the Sheffield HATT blade is presented in Figure 9 and it can be seen that the AoA range between -5° to 5° is the steepest part of the curve which means that for a small change in AoA, a big difference in the lift to drag ratio will occur.

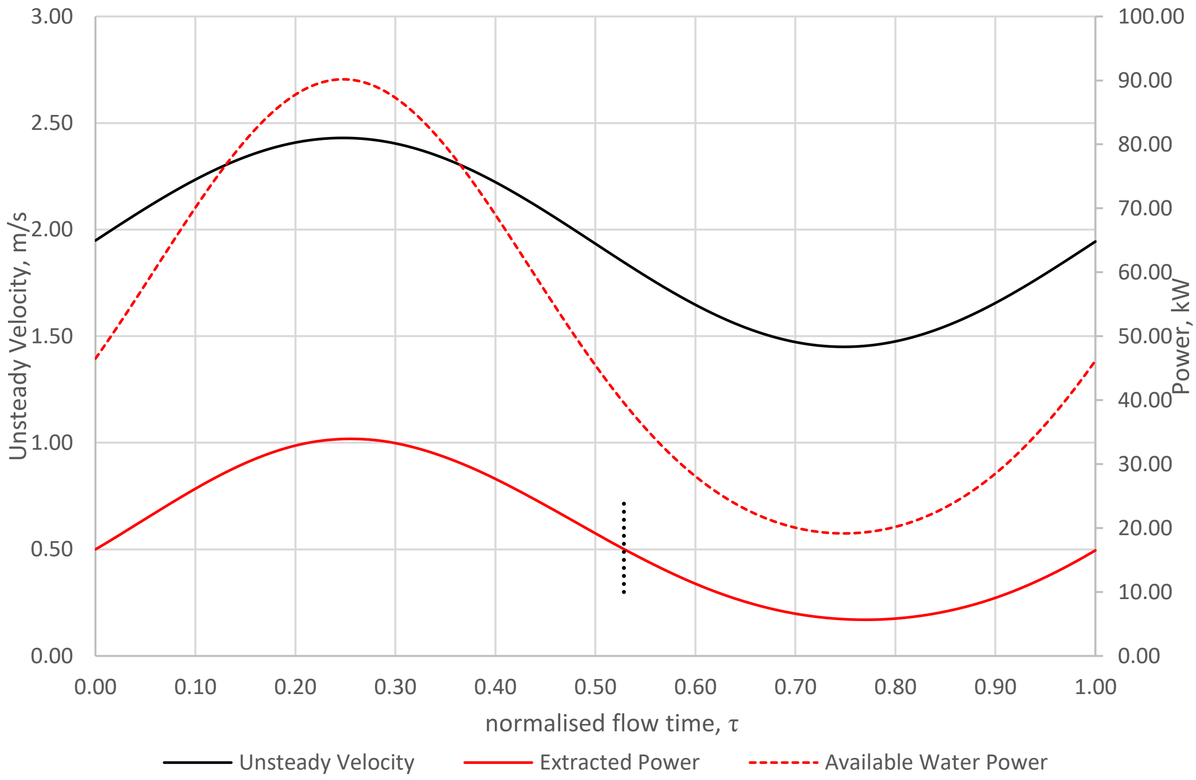

Figure 6a Available water power and extracted power by the turbine with unsteady velocity profile

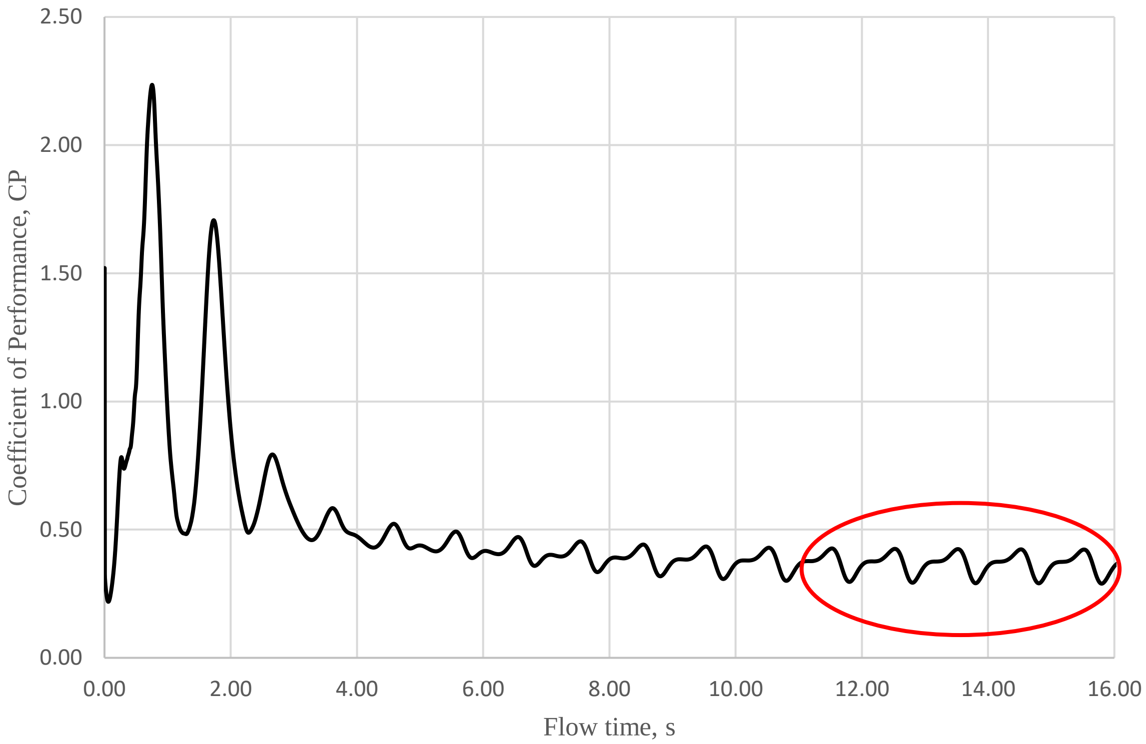

Figure 6b Response of the Sheffield HATT to the unsteady flow scheme implemented

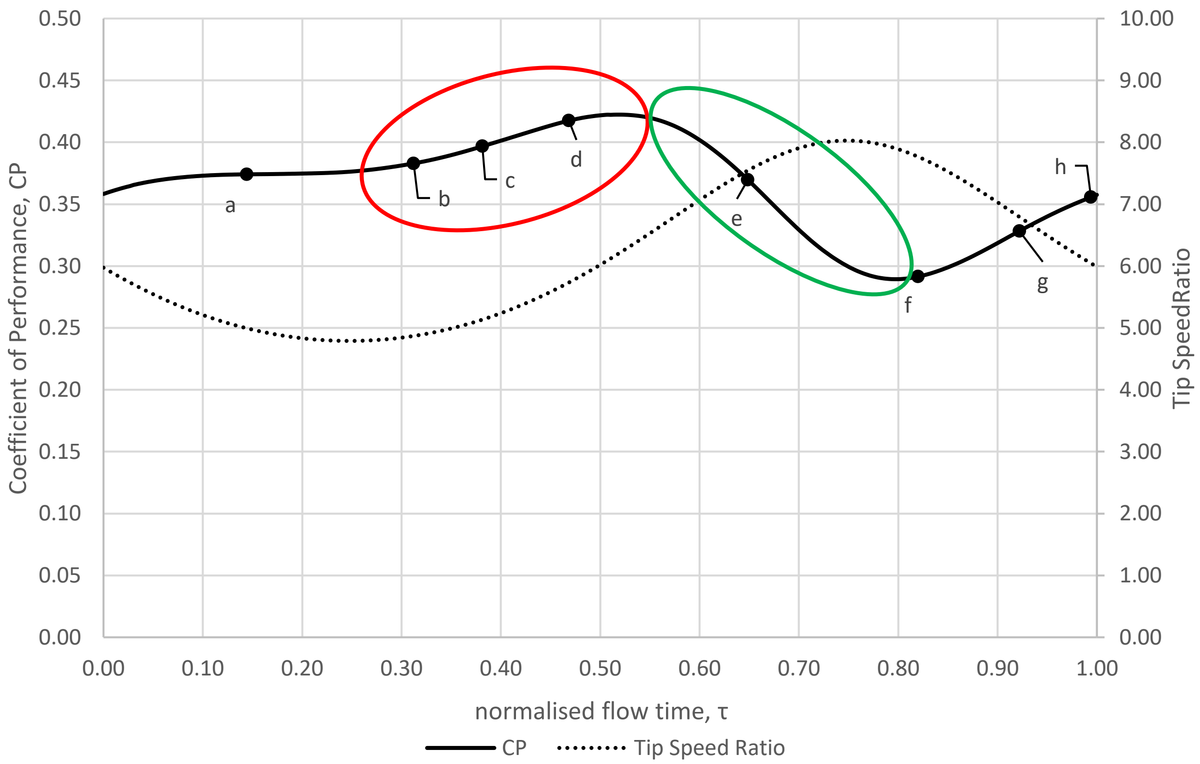

Figure 7 Instantaneous CP curve for one cycle of the unsteady velocity superimposed with the instantaneous TSR

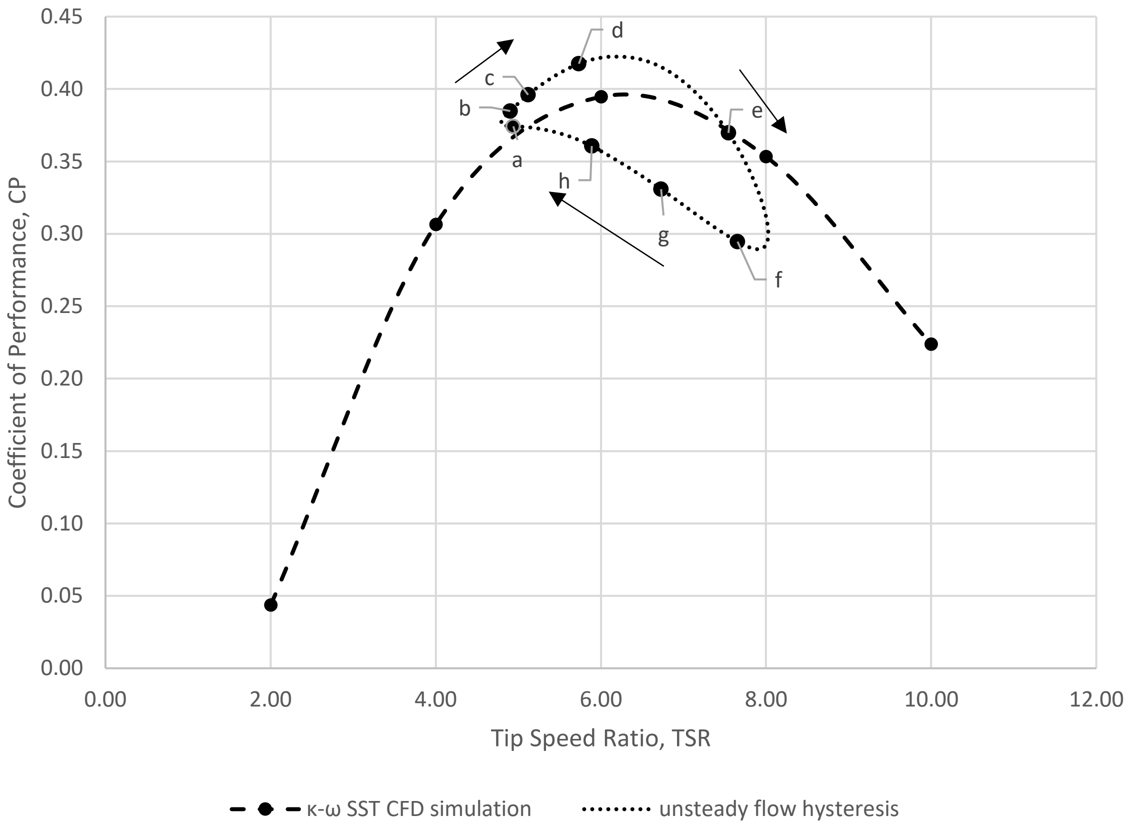

Figure 8 Unsteady flow hysteresis curve for the TSR=6 unsteady simulation over the steady-state performance curve

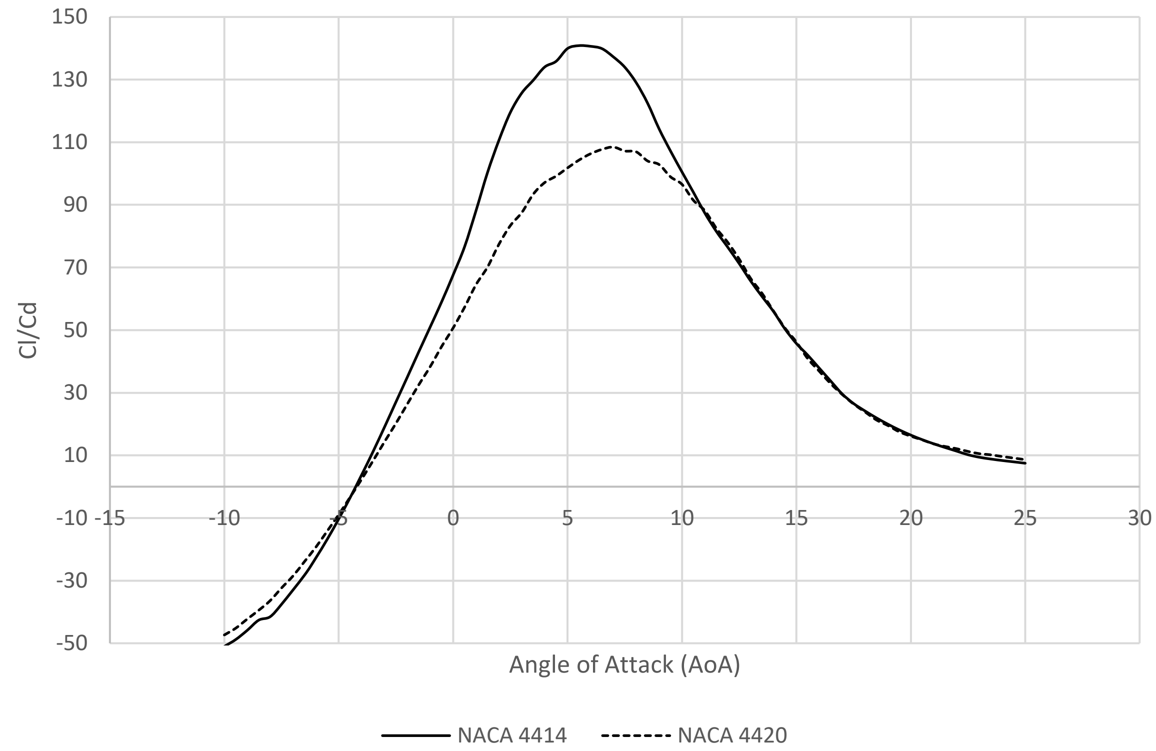

Figure 9 Cl/Cd plot for NACA 4414 and NACA 4420 which are the erofoils at 75% and 25% of the Sheffield HATT blade

Streamlines over the blade at 75% and 25% span are presented in Figure 10. It can be observed how the incident AoA on the hydrofoil sections changes with variation of TSR. For the area highlighted by the oval in the Figure 7, a disturbance in the the streamline in form of a separation was seen at points a, b to c. This is also the area where the delay/lag in the power extracted was observed (as shown in Figure 6) and also where the increase in the instantaneous CP was seen. As the separation reattaches, the instantaneous CP continues to increase until the extracted power starts to decrease after point **d**. It can also be seen from the streamline images that the incident AoA decreases as TSR increases (points **d**, **e** to **f**), suggesting a lower lift although the flow around the blade is fully attached which reflects as a decrease in the instantaneous CP as well. From the lowest CP value of the hysteresis curve near point **f**, it can be seen from the streamline plots that AoA starts to increase and also startes to show evidence of flow separation but the CP values cannot follow the initial path of the curve resulting to different values at same TSR. This illustrates the effect of unsteadiness just as Leishman [29] stated that, in unsteady flow at the same TSR, there will be different values in terms of blade loading and performance, with that of the reattaching flow having higher values when compared to where the flow initially starts the separating part of the process.

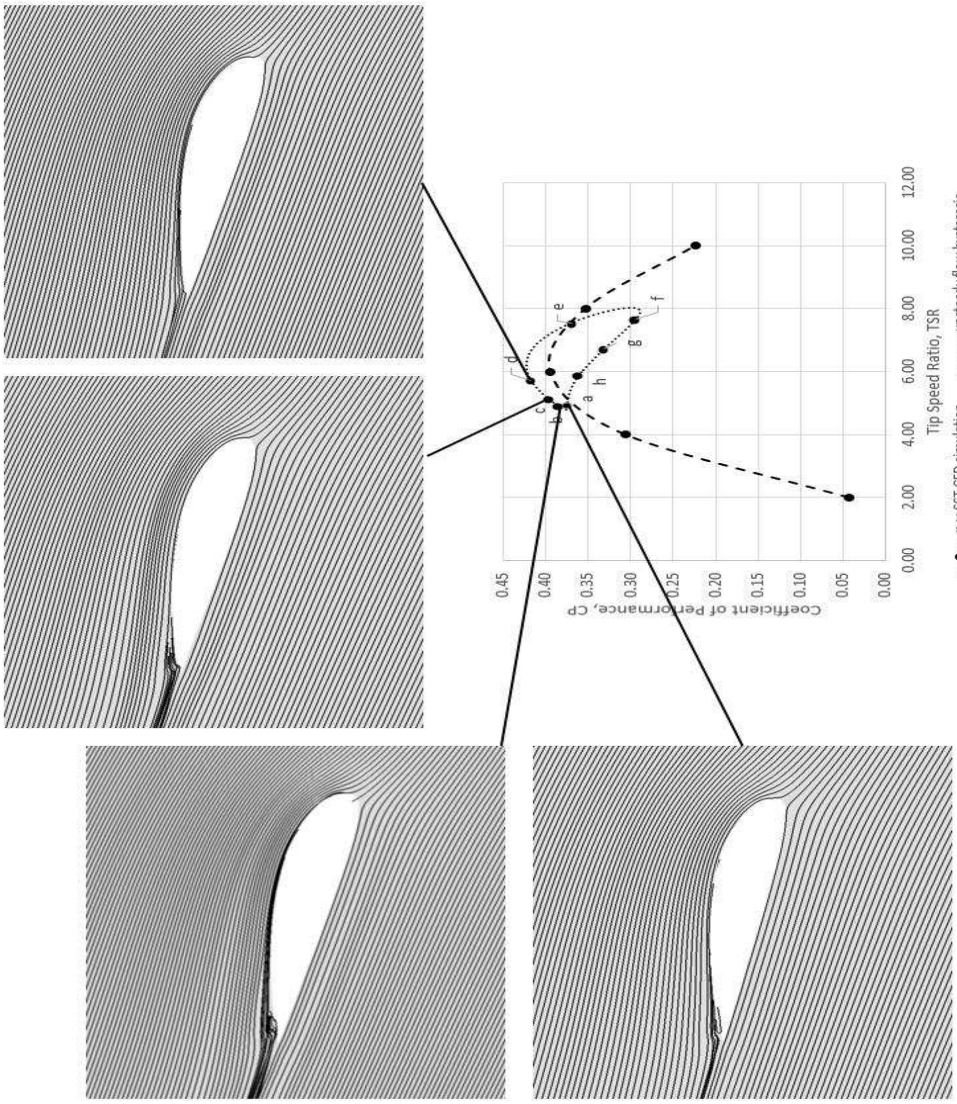

Tip Speed Ratio, TSR
Coefficient of Performance, CP
κ-ω SST CFD simulation
unsteady flow hysteresis
a
b
c
d
e
f
g
h

(a)

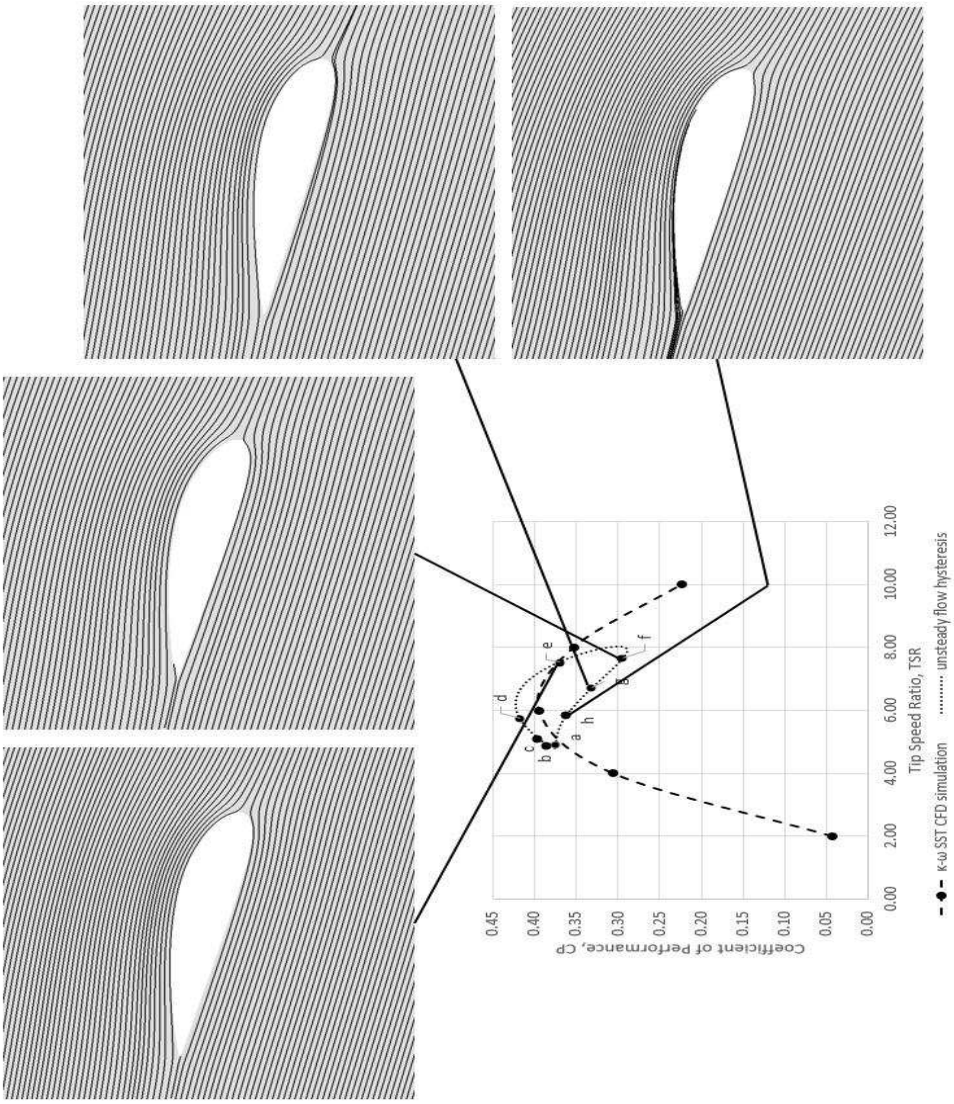

Coefficient of Performance, CP
Tip Speed Ratio, TSR
0.00
0.05
0.10
0.15
0.20
0.25
0.30
0.35
0.40
0.45
0.00
2.00
4.00
6.00
8.00
10.00
12.00
a
b
c
d
e
f
g
h
κ-ω SST CFD simulation
unsteady flow hysteresis

(b)

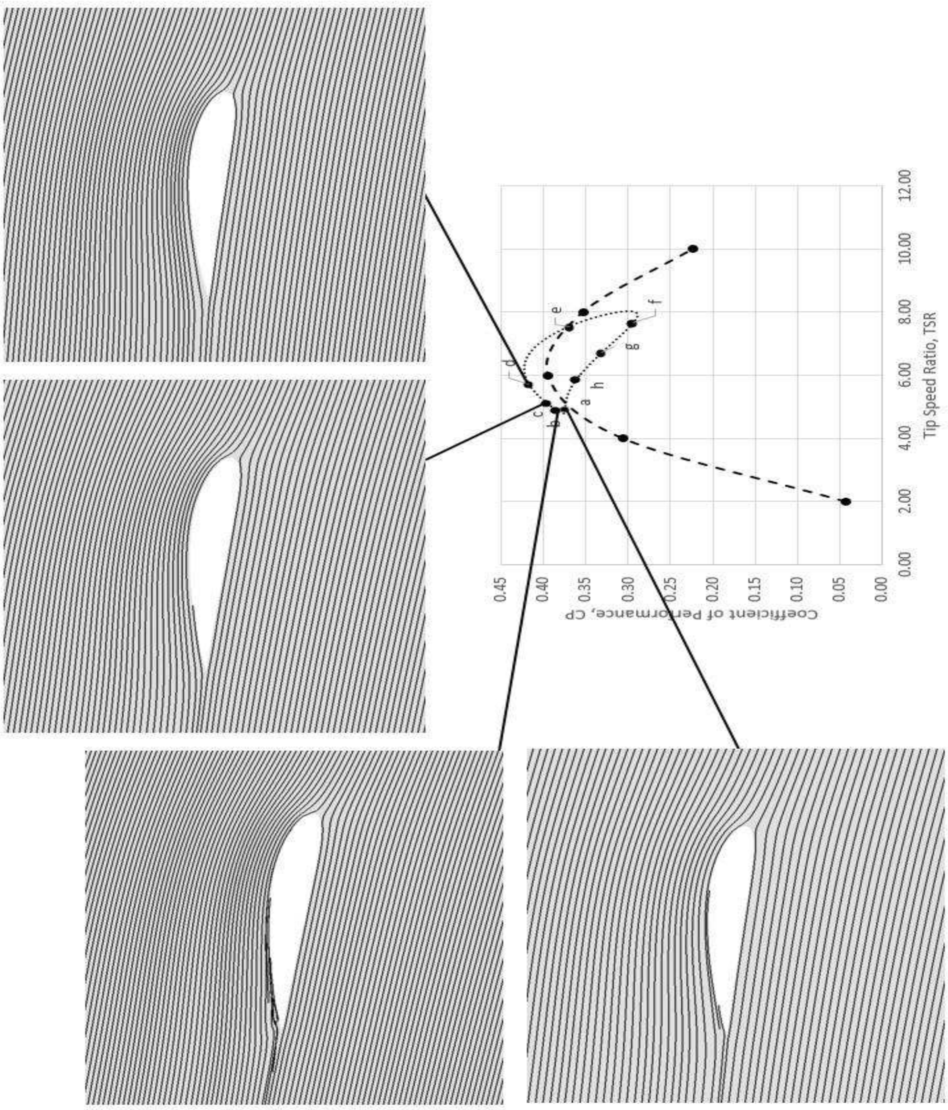

Tip Speed Ratio, TSR
Coefficient of Performance, CP
κ-ω SST CFD simulation
unsteady flow hysteresis

(c)

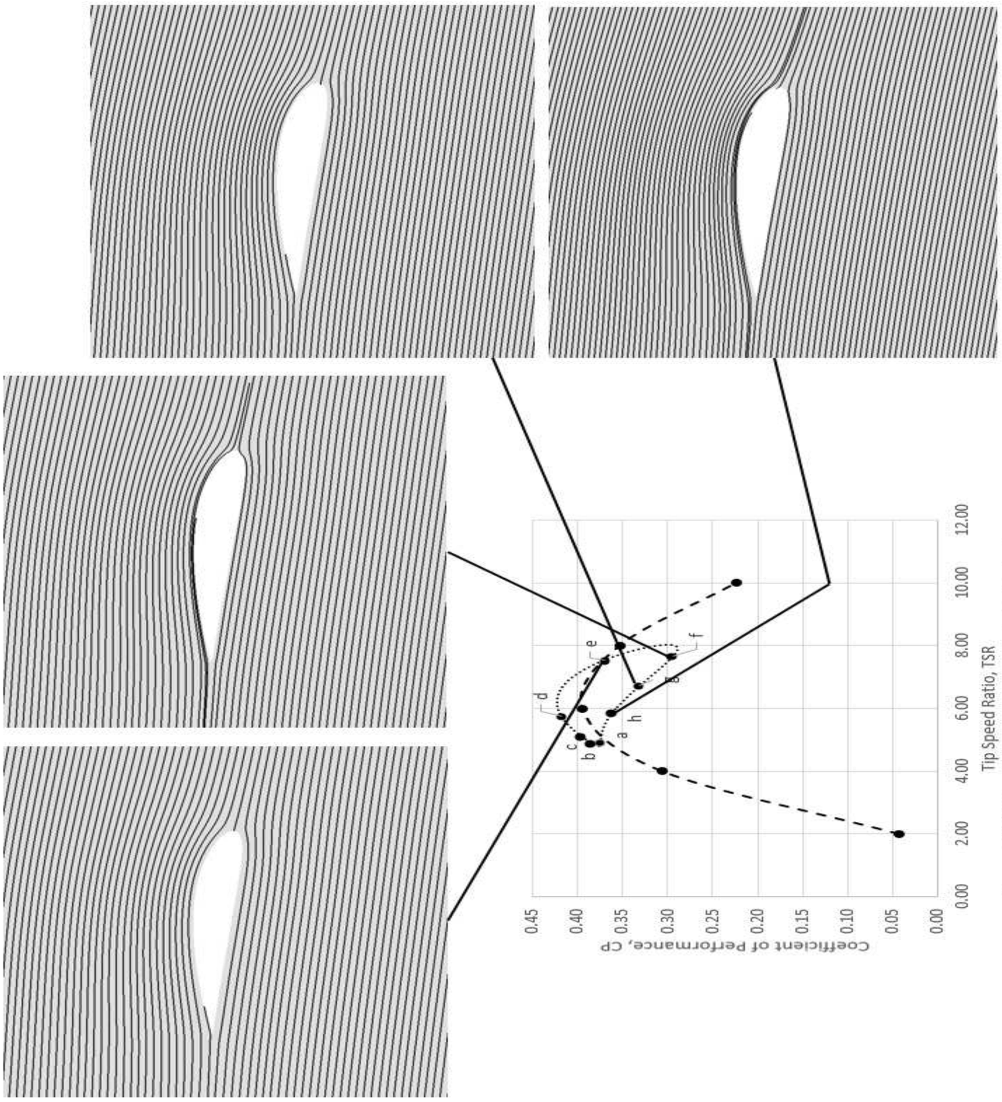

(d)

Figure 10 Streamlines over the hydrofoil sections for the 25% blade span (a and b) and 75% blade span (c and d)

To further understand the response of the turbine to unsteady flow, two unsteady simulations at off-peak TSRs of 4 and 8 were conducted. The equations used to simulate the water speed variation was $u(t) = 1.9402 + 0.49\sin(2\pi t)$ with a rotational velocity of 3.8804 rad/s for the TSR=4 simulation. For the TSR=8 simulation $u(t) = 1.94 + 0.49\sin(2\pi t)$ with a rotational velocity of 7.76 rad/s was used. These maintained the power in the water to be the same as for the steady flow simulations at the same TSR, For the TSR=4 simulation, a cyclic-averaged CP of 22.6% was computed which is 8% lower than its steady state counterpart while a cyclic-averaged CP of 35.1% for the TSR 8 simulation was determined. This is just 0.23% lower than the steady-state CP of 35.33%. The reduced frequency for the two cases are 0.068 and 0.034 respectively.

Shown in Figure 11 are the hysteresis curves for the three unsteady simulations around different TSRs, and illustrates what is happening instantaneously in the flow as the velocity and TSR changes with time. Inspection of the plots shows that each of the curves deviates from the steady-state power curve, although the trend and shape of the hysteresis curves, to an extent, still follows that of the steady-state. For the unsteady simulation around the low TSR, a more drastic separation should be expected, and the λ_2 criterion plot show vortices are present at certain locations around the hysteresis curve as shown in Figure 12. λ_2 is the second in magnitude eigenvalue of the symmetric tensor $\mathbf{S}^2+\mathbf{\Omega}^2$; where $\mathbf{S}$ is the symmetric part of the velocity gradient tensor $\nabla\mathbf{u}$ and $\mathbf{\Omega}$ is the antisymmetric part. The definition given by Jeong and Hussain states that a vortex core is a connected region with two negative eigenvalues of $\mathbf{S}^2+\mathbf{\Omega}^2$. If the eigenvalues are λ_1, λ_2, λ_3 with λ_1 being the smallest and λ_3 the largest, a vortex core can be determined if $\lambda_2<0$[34]. It can be seen that at point **b** in Figure 12, large vortices formed on the suction side of the blade which corresponds to the sudden drop in instantaneous CP curve. Streamline plots at the 75% and 25% blade span for the described time position is presented in Figure 13. At point **c** for the same simulation, it can be seen that the vortices sitting on the suction side of the blade is already dissipating and the flow starts to re-attach, which corresponds to an increase in the instantaneous CP. This observation continued to point **d** where the flow was seen to be fully attached.

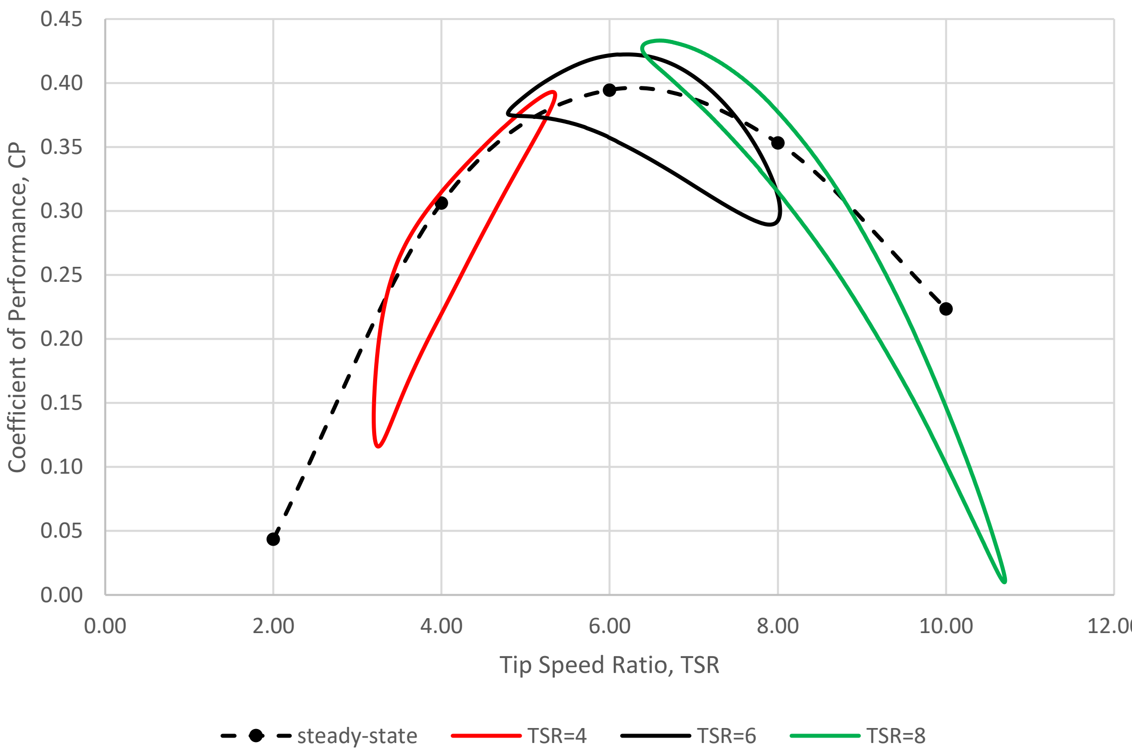

Figure 11 Complete unsteady simulation plot showing hysteresis curves for the three unsteady cases (TSR=4, 6 and 8)

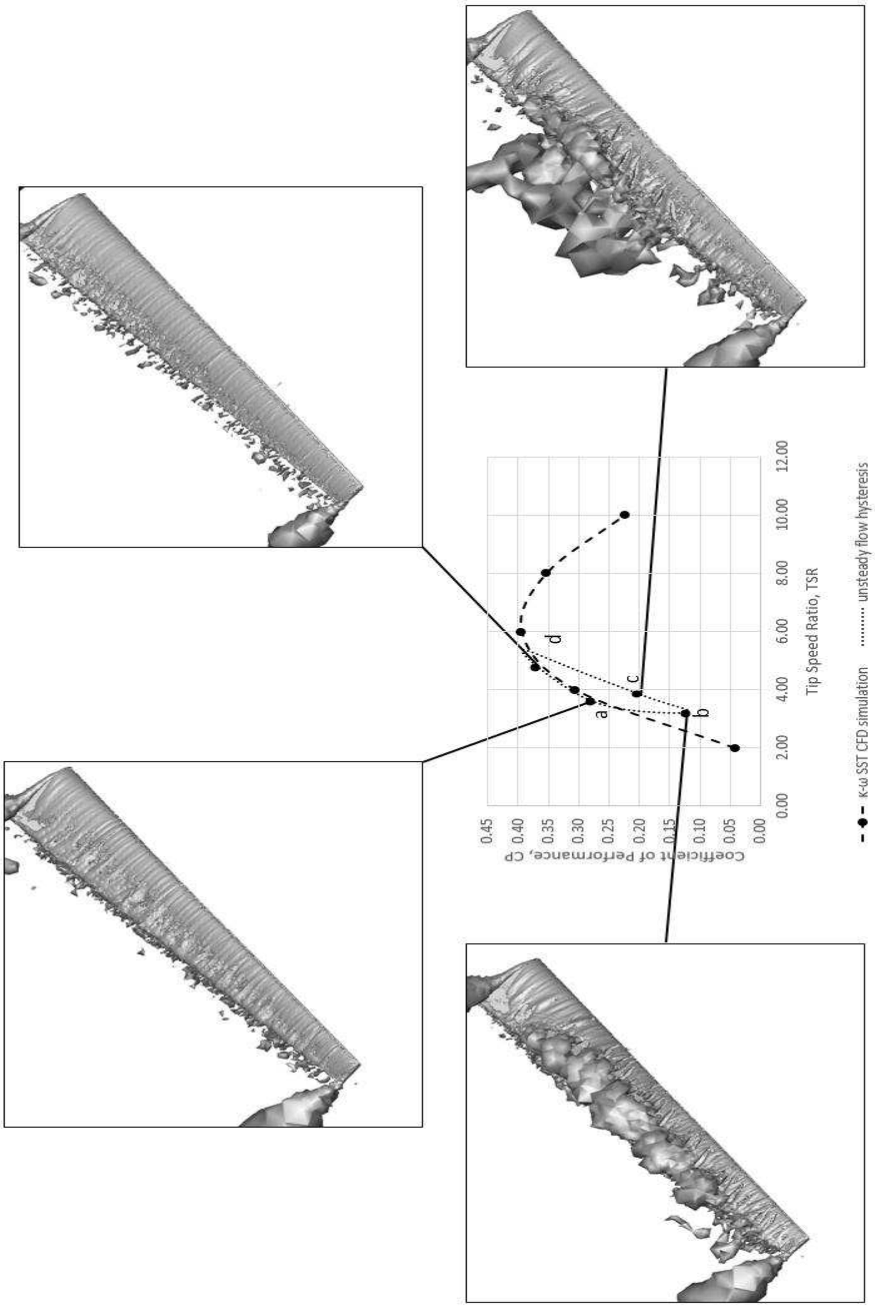

Figure 12 λ_2 criterion vortex tube representation at different points of the unsteady TSR=4 simulation

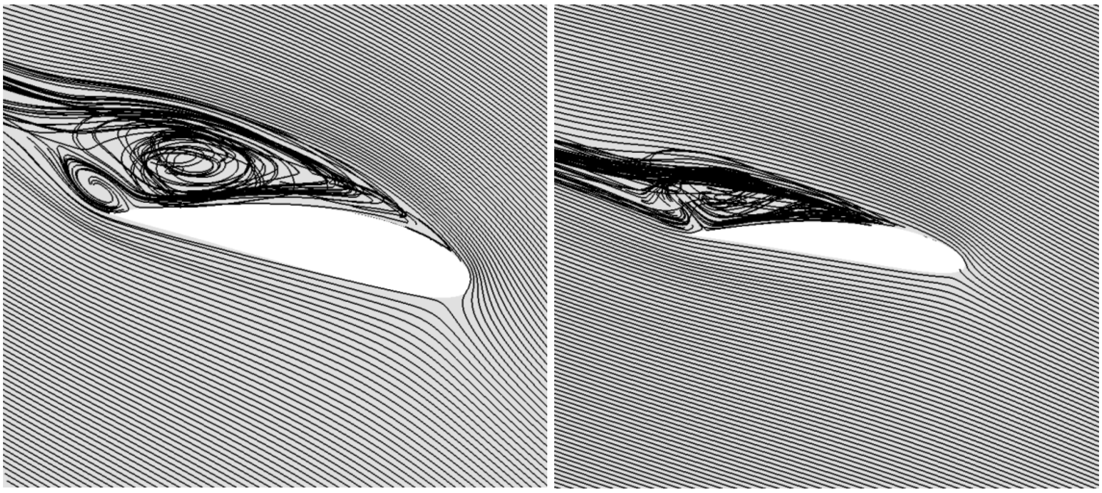

Figure 13 Streamline plots for point b of the TSR=4 unsteady simulation; 25% blade span (left) and 75% blade span (right)

For the unsteady simulation around TSR=8, a narrow but long hysteresis curve was observed, which most closely follows the steady-state power curve and results in a cyclic-averaged CP very close to the steady-state value with only 0.23% difference. The sensitivity of the turbine to small AoA changes is illustrated by this simulation as a large CP variation was observed over a small TSR ranges. Another interesting observation found for this simulation is the region on the hysteresis curve near the optimum TSR that is higher than that of the base case unsteady simulation. This part of the curve makes up for the very low instantaneous CP found for the high TSR region.

3.2 Effects of Amplitude Variation

The influence of amplitude on the performance and the hydrodynamics of the Sheffield HATT is investigated next. The equation used to model the flow was altered so that the resulting amplitude of the velocity variation was set to 10% and 43.5% while again maintaining the cyclic averaged power equal to the steady-state power simulations. The resulting equations are $u(t) = 1.99 + 0.2\ sin(2\pi t)$ and $u(t) = 1.841 + 0.8\ sin(2\pi t)$ for the 10% and 43.5% respectively which also shows that the frequency of the flow was also maintained to be f=1Hz. The results show that for the 10% amplitude simulation, the resulting cyclic-averaged CP is 38.74% which is higher than that of the unsteady base case simulation with a cyclic-averaged CP at 37.5% with a velocity variation amplitude of 24.5% at TSR=6. Although a higher cyclic-averaged CP was obtained, the result is still lower than that of the steady-state CP by 0.72%. For the high amplitude simulation, the cyclic-averaged CP obtained was 34.26% which is 3.24% lower than that of the unsteady base case and 5.2% lower than that of the steady-state CP.

The hysteresis curves for the amplitude variation study simulations are presented in Figure 14 together with that of the steady-state CP curve. The first trend to be seen is that for larger amplitude velocity variation, an increase in the variation in the instantaneous CP was observed especially in the high amplitude simulation hysteresis curve. The hysteresis curve for the 10% amplitude curve is observed to be the smallest and is closest to the steady-state curve which also reflects on the cyclic-averaged CP which is the highest of the three simulations. Also, because the TSR range for the 10% velocity amplitude is small, the high sensitivity of lift to AoA is not so manifest which results in a more oval-shaped curve.

The simulations at high velocity amplitudes show a more dramatic variation in the instantaneous CP especially in the high TSR part of the curve which can again be attributed to the sensitivity of lift of the turbine at low AoA which is observed at high TSR. There are also parts of the hysteresis curve that shows higher instantaneous CP compared to the base case unsteady simulation but those regions with lower CP are larger and this contributes to the lower cyclic-averaged CP overall. It can also be seen that the maximum point of the curves is tending to move to the right as the amplitude increases, this means that the delay in the extracted power in the turbine is extending with increased amplitude. This is probably caused by the separation seen for this simulations, since the TSR range reaches a lower minimum TSR. Figure 15 shows the streamlines for the point highlighted in the high amplitude hysteresis curve (point inside green circle) for both for the 25% and 75% span of the Sheffield HATT where the separation was observed. This is also the start by which the delay in the extracted power manifested and also the start when the instantaneous CP increase. This increase continued as the flow reattaches but because of the delay, the maximum point of the hysteresis curve was shifted to the right at a higher TSR.

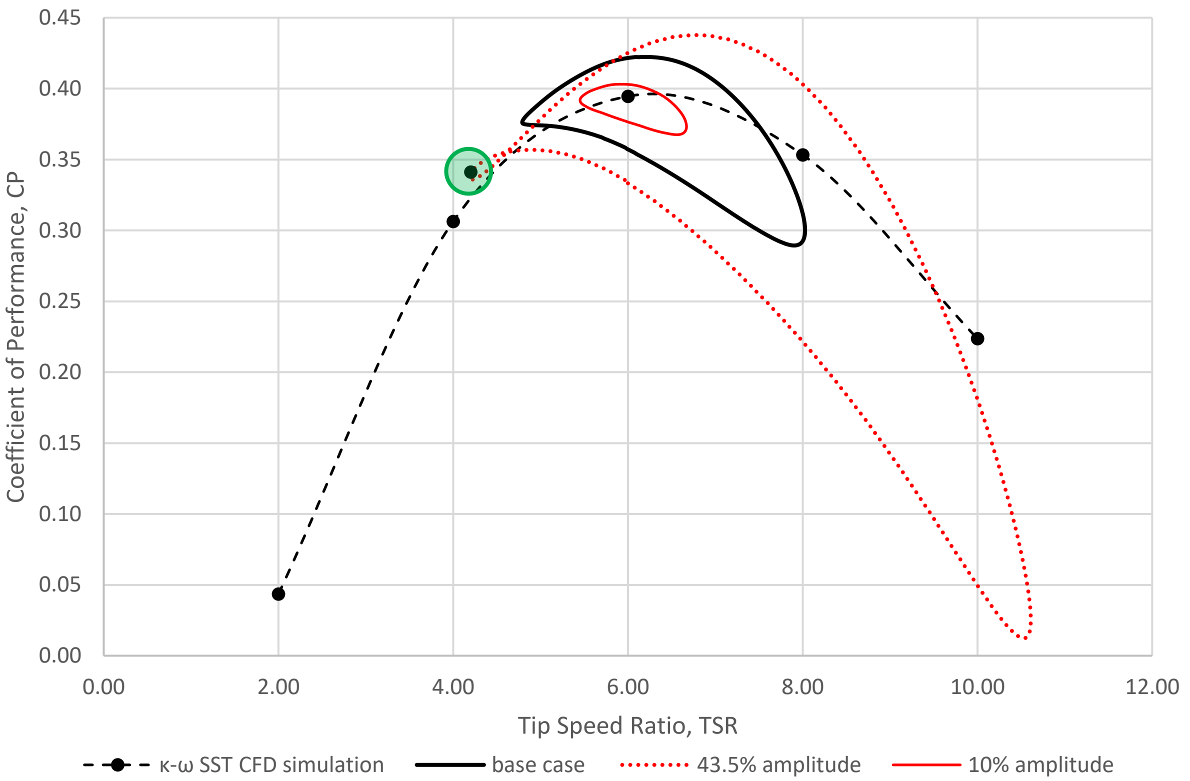

Figure 14 Unsteady flow hysteresis curves for the amplitude variation study

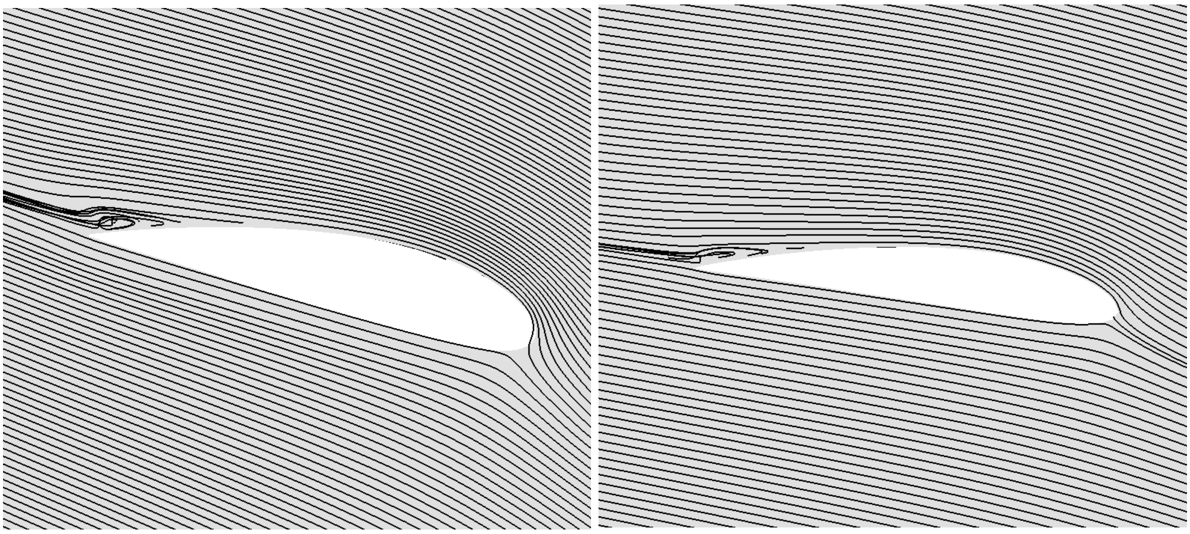

Figure 15 Streamlines over the hydrofoil at the 25% (left) and 75% (right) of the blade at the highlighted point in the high amplitude hysteresis curve

3.3 Effects of Frequency Variation

Two other unsteady simulations were conducted with f=0.5 Hz and f=2.0 Hz, the resulting flow velocity modelled as $u(t) = 1.94 + 0.8 \sin(\pi t)$ and $u(t) = 1.841 + 0.8 \sin(4\pi t)$. A cyclic-averaged CP of 37.9% was obtained from the low frequency simulation which is higher than the unsteady base case simulation by 0.4% but still lower than that of the steady-state CP by 1.56%. The unsteady base case here is that at f=1, A=24.5% and TSR=6. On the other hand, the high frequency simulation yields a cyclic-averaged CP of 37.11% which is now lower than that of the base case by 0.39%. All unsteady simulations have a lower CP than the steady-state simulation, clearly suggesting the detrimental effect of unsteadiness. It is also the case that as the frequency decreases, the cyclic-averaged CP became closer to the steady-state CP. It was shown in this study that the effect of unsteadiness decreases with frequency but still, there is a clear effect of unsteadiness in terms of performance.

The resulting hysteresis curves for the frequency variation study is presented in Figure 16. The f=0.5 Hz simulation produced a hysteresis curve that is thinner than that of the base case (f=1.0) but still similar in shape indicating the aerodynamics are similar. It is also clear that the hysteresis curve is the closest to the steady-state power curve in terms of shape, trend and value. The hysteresis curve for the f=2.0 simulation is the first to show a different shape when compared to all of the other hysteresis curves presented in this paper and indicates a fundamental change in aerodynamics. It shows a more rounded curve with maximum instantaneous CP happening at a later TSR near 7 suggesting that the delay or lag observed in this case is longer than that of the base case. It is suggested that this means that the turbine is never in equilibrium with the flow because the reduced frequency for this case is high at a value of 0.1021 (the ratio of the flow frequency to the rotational frequency is at 2.16.) The significant drop at high TSR was still observed although the recovery region for the instantaneous CP was almost just a flat line and the increase only started when the curve was at the low TSR region as the flow reattaches after some separation was observed in the same region.

Additional simulations at higher frequency (f=3.0 and f=4.0) were conducted. Results obtained showed that the cyclic-averaged CP are 36.8% and 37.11% for the f=3.0 and f=4.0 unsteady simulations, which are very close to that of the f=2.0 case. This suggests that there is a limit, in terms of frequency, by which the unsteadiness of the flow affects performance. Figure 16 shows that the summary of performance in terms of flow frequency for the Sheffield HATT and it can be seen that before f=2.0, the trend of the plot shows a decrease in cyclic-averaged CP as frequency increases but from f=2.0 onwards, the values does not continued to decrease and maintained value near that of the f=2.0 simulation.

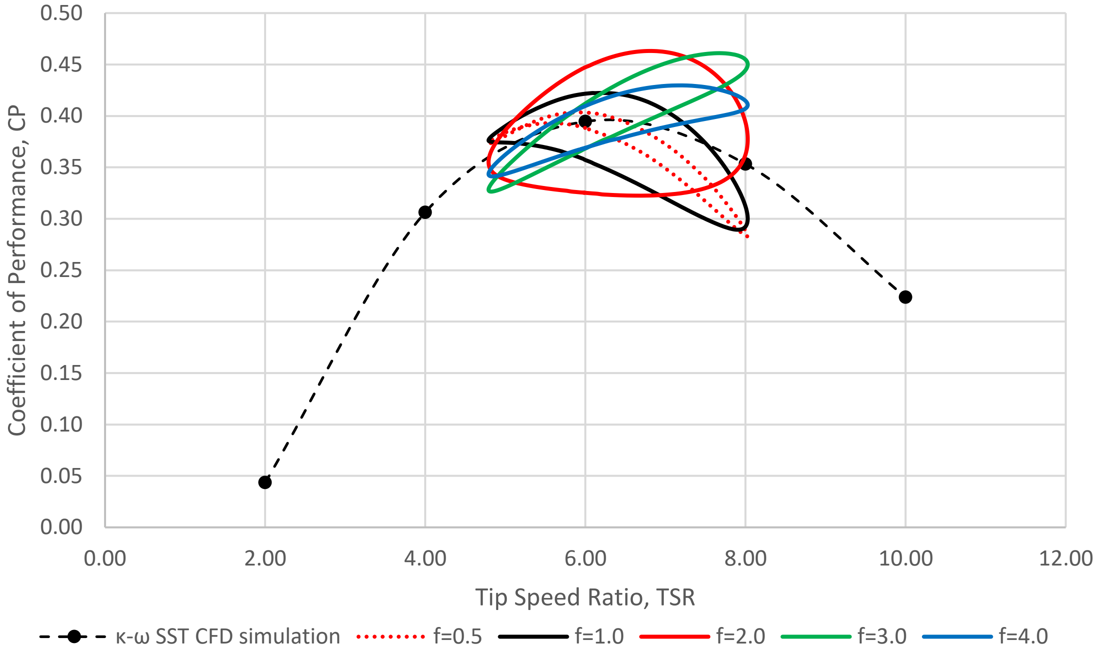

Figure 16 Unsteady Flow Hysteresis Curve for the Frequency Variation Study

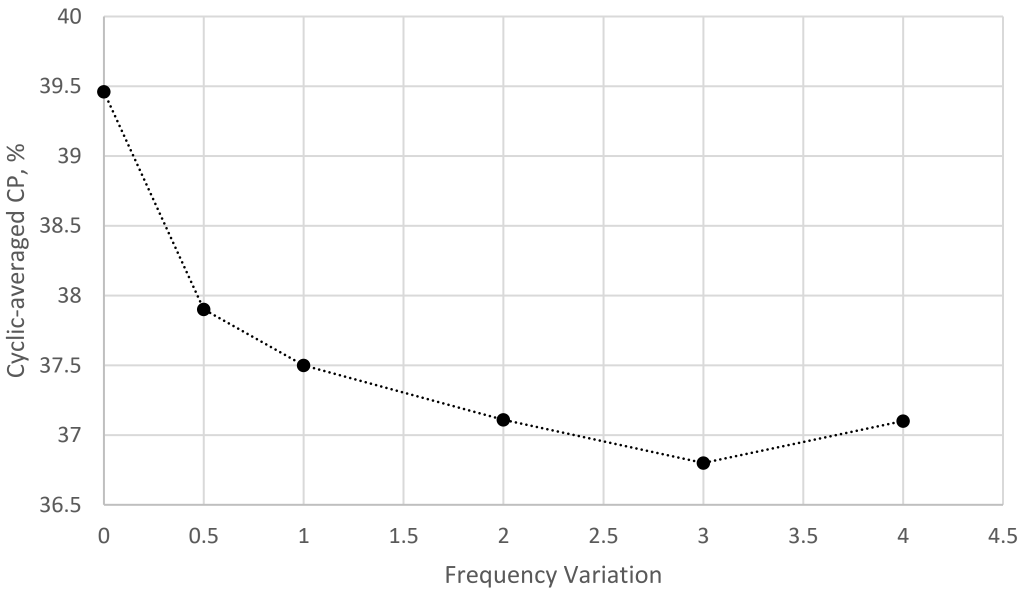

Figure 17 Summary of the performance of the Sheffield HATT in unsteady flow in terms of frequency with the f=0 mark being the steady-state CP

4. CONCLUSIONS

This study presented the performance of the Sheffield HATT both in steady and unsteady flow. The unsteady cyclic-averaged CP at optimum TSR was shown to be 37.50% which is lower than the maximum steady flow CP at 39.46%. A hysteresis curve was observed for the unsteady simulation that is shown not to follow the steady-performance curve. This hysteresis is caused by a delay that was observed for the extracted power plot for the turbine in unsteady flow showing that the first part of the cycle is not the same as the second half and thus resulting to an asymmetrical CP response. The physics explaining the phenomenon was shown to be caused by inertia effects affecting the lift and drag at different parts of the unsteady flow cycle.

Unsteady simulations away from peak TSRs are also presented which shows that the unsteady cyclic-averaged CP is still lower than their steady flow counterpart. A difference of 8.0% was seen from the TSR=4 unsteady simulation, while a smaller difference (0.23%) was observed for the TSR=8. This results in a trend showing that, as the mean TSR increases, the cyclic-averaged CP gets closer to the corresponding steady flow CP. This can be attributed to the more drastic separation seen at low TSR which is shown to be dependent on the reduced frequency.

The effect of amplitude on performance was shown to be relatively linear where a decrease cyclic-averaged CP was observed as the amplitude of the unsteady equation was increased. A cyclic-averaged CP of 38.74% was observed for the 10% amplitude simulation while 34.26% was recorded for the 43.50% amplitude simulation.

In terms of the frequency variation study, the low amplitude unsteady simulation at f=0.5 Hz shows a higher cyclic-averaged CP at 37.9% which is 0.4% higher than that of the base case simulation at f=1Hz. A thinner and smaller hysteresis curve was observed for this case showing a very small variation on the instantaneous CP thus resulting to a higher cyclic-averaged CP. As the frequency was increased to f=2.0 Hz, f=3.0 Hz and f=4.0 Hz, the cyclic-averaged CPs obtained were 37.11%, 36.8% and 37.1% respectively. This shows a decrease in the cyclic-averaged CP as the frequency increases although the variation is smaller when compared to the amplitude variation study especially in the high frequency cases.

Overall, it was shown that for all of the unsteady cases presented, the cyclic-averaged CP of the Sheffield HATT is lower than the steady state reference case suggesting that the presence of unsteadiness in the velocity inflow is detrimental to the performance of this turbine.

ACKNOWLEDGEMENTS

The authors would like to thank the Department of Science and Technology (DOST) – Engineering Research and Development for Technology (ERDT) for the funding provided in the form of the faculty development grant.

REFERENCES

[1] Marine Turbines (2017, January) Retrieved from Marine Turbines: http://www.marineturbines.com/Tidal-Energy
[2] Bahaj A. (2012), New Research in Tidal Current Energy, Philosophical Transactions of the Royal Society A, DOI:10.1098/rsta2012.0501.
[3] King, J., & Tryfonas, T. (2009). Tidal Stream Power Technology - State of the Art. IEEE.
[4] EMEC. (2017, January). Alstom (Formerly TGL). Retrieved from EMEC: http://www.emec.org.uk/about-us/our-tidal-clients/alstom/
[5] Bahaj, A., Batten, W., & McCann, J. (2007). Experimental verifications of numerical predictions for the hydrodynamic performance of horizontal axis marine current turbines. Renewable energy, 2479-2490.
[6] Chamorro, L., Hill, C., Morton, S., & Ellis, C. (2013). On the interaction between a turbulent open channel flow and an axial-flow turbine. Journal of Fluid Mechanics, 658-670.
[7] Walker, S. (2014, November). Hydrodynamic interactions of a tidal stream turbine and support structure. PhD Thesis. University of Sheffield.

[8] Morris, C. (2015). Influence of Solidity on the Performance, Swirl, Characteristics, Wake Recovery and Blade Deflection of a Horizontal Axis Tidal Turbine. PhD Thesis. Cardiff University.

[9] Batten, W., Bahaj, A., Molland, A., & Chaplin, J. (2007). Experimentally Validated Numerical Method for the Hydrodynamic Design of Horizontal Axis Tidal Turbines. Ocean Engineering, 1013-1020.

[10] Danao, L., Abuan, B. and Howell, R. (2016) Design Analysis of a Horizontal Axis Tidal Turbine, 2nd Asian Wave and Tidal Conference. Marina Bay Sands, Singapore.

[11] Abuan, B. and Howell, R. (2016). Effect of Idealised Unsteady Flow to the Performance of Horizontal Axis Tidal Turbine, 2nd Asian Wave and Tidal Conference. Marina Bay Sands, Singapore.

[12] Malki, R., Williams, A., Croft, T., & Masters, I. (2013). A coupled blade element momentum - Computational fluid dynamics model for evaluation of tidal stream turbine performance. Applied mathematical Modelling, 3006-3020.

[13] MacLeod, A., Barnes, S., Rados, K., & Bryden, I. (2002). Wake effects in tidal current turbine farms. Proceedings from Inernational Conference of Marine Renewable Energy. Newcastle.

[14] Mason-Jones, A., O'Dohetry, D., Morris, C., & O'Dohetry, T. (2013). Influence of a velocity profile & support structure on tidal stream turbine performance. Renewable energy, 23-30.

[15] O'Dohetry, T., Mason-Jones, A., O'Dohetry, D., Evans, P., Wooldridge, C., & Fryett, I. (2010). Considerations of a horizontal axis tidal turbine sited off the Welsh coast. 8th European Wave and Tidal Conference.

[16] Afgan, I., McNaughton, J., Rolfo S., Apsley, D., Stallard, T., & Stansby, P. (2013). Turbulent flow and loading on a tidal stream turbine by LES and RANS. International Journal of Heat and Fluid Flow, 96-108.

[17] Kang, S., Borazjani, I., Colby, J., & Sotiropoulos, F. (2012). Numerical simulation of 3D flow past a real-life marine hydrokinetic turbine. Advances in Water Resources, 33-43.

[18] O'Rourke, F., et al.,(2015) Hydrodynamic performance prediction of a tidal current turbine operating in non-uniform inflow conditions, Energy, 93, pp 2483-2496

[19] Ai, K., et. al., (2016) Surface wave effects on marine current turbine, modeling and analysis, Proceedings of 2016 7th International Conference on Mechanical and Aerospace Engineering, pp 180-184.

[20] Leroux, T., Osbourne, N., McMillan, J., Groulx, D., & Hay, A. (2016). Numerical Modelling of a TIdal Turbine Behaviour under Realistic Unsteady Tidal Flow. 3rd Asian Wave and TIdal Conference. Marina Bay Sands, Singapore.

[21] de Jesus Henriques, et al, (2016) The influence of blade pitch angle on the performance of a model horizontal axis tidal stream turbine operating under wave-current interaction, Energy, 106, pp. 166-175.

[22] Gant, S., & Stallard, T. (2008). Modelling a tidal turbine in unsteady flow. Proceedings from Offshore and Polar Engineering Conference. Vancouver.

[23] Milne, I., Day, A., Sharma, R., & Flay , R. (2016). The characterisation of the hydrodynamic loads on tidal turbines due to turbulence. Renewable and Sustainable Energy.

[24] Young, Y., Motley, M., & Young , R. (2010). Three-Dimensional Numerical Modelling of the Transient Fluid-Structural Interaction Response of Tidal Turbines. Journal of Offshore Mechanics and Arctic Engineering.

[25] Miniaci, D. (2012). Investigating the Influence of the Added Mass Effect to Marine Hydrokinetic Horizontal-Axis Tidal Turbines Using a General Dynamic Wake WInd Turbine Code. Marine Technology Society Journal.

[26] Whelan, J. I. (2010). A fluid dynamic study of free-surface proximity and inertia effects of tidal turbines. PhD Thesis. Imperial College of Science, Technology and Medicine.

[27] Milne, I., Day, A., Sharma, R., & Flay, R. (2012). Blade loads on tidal turbines in planar oscillatory flow. Ocean Engineering, 163-174.

[28] Lee, T., & Gerontakos, P. (2004). Investigation of flow over oscillating airfoil. Journal of Fluid Mechanics, 313-341.

[29] Leishmann, J. G. (2006). Principle of Helicopter Aerodynamics. Cambridge University Press.

[30] McNae, D. (2014). Unsteady hydrodynamics of Tidal Stream Turbines. PhD Thesis. Imperial College London.

[31] Galloway, P. (2013). Performance Quantification of Tidal Turbines Subjected to Dynamic Loading. PhD Thesis. University of Southampton.

[32] Luznik, L., Flack, K. A., Lust, E. E., & Taylor, K. (2013). The effect of surface waves on the performance characteristics of a model tidal turbine. Renewable Energy.

[33] Carbon Trust. (2005). United Kingdom Wave and Tidal Energy Study. Variability of UK Marine Resources.

[34] Jeong J. and Hussain F. (1995). On the identification of a vortex, Journal of Fluid Mechanics, 285:69-94.

[35] Abuan, B.E. (2017) The Performance and Hydrodynamics in Unsteady Flow of a Horizontal Axis Tidal Turbine, PhD Thesis, accessible online at whiterose.ac.uk